Available online at www.sciencedirect.com
SCIENCE DIRECT
Polymer 46 (2005) 7323–7333
polymer
www.elsevier.com/locate/polymer

Maleated and non-maleated polyethylene–montmorillonite layered silicate blown films: creep, dispersion and crystallinity

Ajit Ranade[a], Kasinath Nayak[b], Debora Fairbrother[c], Nandika Anne D'Souza[a,*]

[a]*Department of Materials Science and Engineering, University of North Texas, P.O. Box 305310, Denton, TX 76203, USA*
[b]*Huntsman LLC, Odessa, TX 79760, USA*
[c]*NASA Wallops Flight Facility, Wallops Island, VA 23337, USA*

Received 1 August 2004; received in revised form 24 March 2005; accepted 7 April 2005
Available online 15 July 2005

Abstract

Non-linear time dependent creep of polyethylene (PE) montmorillonite layered silicate (MLS) nanocomposites was investigated. PE grafted maleic anhydride (PE-*g*-MA) was used, as a coupling agent to improve the miscibility between PE and organically modified MLS. The creep and tensile response of maleated and non-maleated PE nanocomposites were determined. Tensile properties of maleated PE nanocomposites were higher than the non-maleated nanocomposites. Non-linearity in the creep response was modeled using the Burger model. A drop in the retardation time was observed for maleated PE nanocomposites. XRD, polarized optical microscopy and a differential scanning calorimeter (DSC) were used to probe crystallinity and clay dispersion in the films. The tensile and creep properties were related to dispersion due to presence of MLS. The deformation response of PE blended with PE-*g*-MA and each of these separately modified by MLS showed synergistic contributions of the constituents. The response was attributed to dispersion effects with marginal effects of crystallinity.

Keywords: Burger model; Non-linear creep; PE nanocomposites

1. Introduction

In recent years, different organic or inorganic modifiers have been used to improve the mechanical, chemical and rheological properties of polymers. Linear low-density polyethylene film has been used in the fabrication of high altitude scientific research balloons for decades. The stratospheric environment in which the balloons fly requires the materials to be ductile down to −90 °C which limits the materials that can be used. As scientific ballooning transitions to pressurized balloon systems, materials with increased strength and decreased deformation under constant load are desired. Separately, polymer-inorganic montmorillonite layered silicate (MLS) mixtures have become extremely popular over the last decade for a variety of reasons. Since, the reinforcing element has one dimension in the low nanometer range, the systems are referred to as nanocomposites. Improvement in the mechanical properties (doubling of tensile modulus and strength), improved barrier properties, improved flame retardance, increased dimensional stability, and improvement in the heat distortion temperature (up to 100 °C) [1–4] have all been determined in various systems, sometimes concomitantly. Increased interfacial area of the layered silicates has led to attractive results at very low MLS loading (2–3% by weight). In some systems, no decrease in optical transmission was reported [2]. It is clear that dispersion and the concentration of dispersed phase plays a crucial role in the properties of polymer nanocomposites. A comparative assessment of the properties obtained in nanocomposites reveals an essential fact: smaller the dispersed phase, and more homogeneously the dispersion, higher the improvement of physical and mechanical properties. Increased specific interactions between the polymer and the clay are, therefore, vital. This is engineered by functionalization of the layers with surfactants such as alkyl ammonium surfactants. The influence of clay treatment on the dispersion has driven much of the earlier research. Nanocomposites of polyethylene have not been the subject of extensive investigation given that the non-polar

* Corresponding author. Tel.: +1 940 565 2979; fax: +1 940 565 4824.
E-mail address: ndsouza@unt.edu (N.A. D'Souza).

0032-3861/$ - see front matter © 2005 Elsevier Ltd. All rights reserved.
doi:10.1016/j.polymer.2005.04.085

nature of the base unit makes miscibility with the MLS difficult. The correlations between creep below the melting point of nanocomposites and potential effects of crystallization and dispersion have not been probed.

Creep has been investigated in the melt regime for other olefin clay based nanocomposites. Lele et al. [5] investigated creep in PP nanocomposites compatibilized and not compatibilized with maleated PP. They found increased creep resistance and an increase in zero shear viscosity (3-fold) of PP nanocomposites. The compatibilizer played a significant role in the increase. The rheological response of layered silicate nanocomposites was determined to arise from frictional interactions between the silicate layers and not due to immobilization of confined polymer chains between the silicate layers. Wang et al. [6] observed an increase in storage modulus, loss modulus and dynamic viscosities in PP melt with increase in clay content. The rise in values was related to the confinement of PP chains in the presence of MLS and strong hydrogen bonding between polar groups of maleic anhydride and oxygen groups of MLS. Thus while both Lele et al. [5] and Wang et al. [6], observed the same effects of increased melt elasticity, the reasoning attributed to this increase differed. Lim et al. [7] studied the viscoelastic properties of aliphatic biodegradable polyester nanocomposites melt. In an oscillatory mode, the frequency dependence of storage and loss modulus decreased monotonically with clay content. An increase in zero shear rate viscosity and shift of the crossover point (storage modulus vs. loss modulus) to a lower frequency was observed with increase in MLS content. Pegoretti et al. [8] studied creep properties of polyethylene terephthalate (PET) nanocomposites in solid state (dumb-bell shape specimens). They found an increase in creep resistance properties in PET nanocomposites. Long term creep properties of PET nanocomposites also showed improvement compared to neat PET. Lee et al. [9] studied the viscoelastic properties of epoxy nanocomposites. They found an increase in relaxation time in cured epoxy nanocomposites. This was related to uniform dispersion of the MLS at molecular and microscopic levels.

In investigating PE nanocomposites, the creep response in the solid state is of vital interest given that it is used above its glass transition temperature. Unlike amorphous polymers, the viscoelastic response of a semicrystalline polymer like PE cannot generally be treated using time temperature superposition. There are several reasons for this. First, the crystallites in the material exhibit relaxations having different temperature dependencies than the amorphous phase. Second, the amorphous phase in the semicrystalline polymer may be changed by the presence of the crystallites. The non-linear time dependent response of polyethylene has been a focus of attention for many years. Lai et al. [10] studied short term and long term creep effects of high density polyethylene. They found a change in the relaxation time even under low stresses. Prior efforts from our laboratory showed decreased creep response with addition of MLS in polypropylene (PP) [11]. A high degree of non-linearity was observed at low stresses and the aging behavior was independent of stress. The results obeyed the time-elapsed time superposition suggested by Struik for semicrystalline polymers. Ward [12] showed the existence of two yield points in isotropic PE. The first yield point is related to a rapid decrease in strain rate at low strains. The second yield point is characterized by significant necking of the sample to produce permanent plastic flow. Ward used two models, the two process model of Wilding and Ward [13] and co-operative jump model of Fortheringham and Cherry [14], to explain the two yield behavior and found the two process model fit better than the cooperative model. Zhang et al. [15] studied the non-linear behavior of HDPE under uniaxial compression. Under loading and unloading conditions, stress–strain relations were found to be highly non-linear and dependent on both strain and strain rate. The permanent strain observed during the creep test was related to the loading history, maximum strain applied, strain rate and the time during which material were steadily deformed. Zhang et al. [16] continued their work on non-linear behavior of HDPE under uniaxial compression. They developed a non-linear viscoelastic and viscoplastic constitutive model. The non-linear viscoelastic model predicted the material behavior reasonably well at low loading conditions. Suwanprateeb et al. [17] investigated the creep behavior in PE and hydroxyapatite reinforced PE. The creep resistance increased with volume fraction of hydroxyapatite. The increase in creep resistance was associated with an increase in modulus. The failure in composites at longer time intervals was related to decoupling at the hydroxyapatite PE interface. Rand et al. [18] subjected PE films to different stresses and temperatures. Master curves of PE films from dynamic mechanical analysis (DMA) used in conjunction with non-linear functions accurately predicted the response of PE. They used constitutive equations discussed by Schapery [19] to study the non-linear behavior of PE films. Rand et al. [18] found the reduced time Ψ and amplitude of the compliance is a function of both stress and temperature and there exists a proportional limit at each temperature below which the material behaves as a linear viscoelastic material. The principles of time temperature superposition used in non-linear viscoelastic characterization were found insufficient to use in PE films at most stress levels of interest. Zhou et al. [20] studied the creep behavior of melt extruded HDPE films, having stacked lamellar morphology and compression molded slow cooled isotropic films of the same resin. An Eyring rate model was used to analyze the creep data, and the three parameters associated with the Eyring rate model, i.e. activation volume, activation energy, and the availability of creep sites. It was observed that the creep behavior of all the films was basically controlled by the deformation of the amorphous phase and more specifically, by the density and tautness of tie chains. Xu et al. [21] blended high creep PE with low creep polystyrene. They found

improved creep resistance in PE/PS blend compared to pure PE. The creep resistance was dependent on concentration of PS and type of processing. Hubert et al. [22] showed improved creep resistance in ethylene/α-olefin blends with a bimodal molecular weight distribution compared to unimodal copolymers of same crystallinity. The bimodal polymer showed evidence of greater chain entanglement and tie chain densities compared with unimodal copolymers. The physical network of crystalline lamellae (creep of isotropic materials) or microfibrils (drawn materials) bound by tie chains and entangled chain loops, was related to the mechanical strength. Drozdov et al. [23] derived the constitutive equation for the time dependent behavior of semicrystalline PE. Their creep tests showed standard viscoelastic and viscoplastic behavior of semicrystalline polymers. They also observed fair agreement between the experimental data and the results of numerical simulation.

It is clear, therefore, that the non-linear effects in polyethylene, consequences of MLS addition, correlation to dispersion of the MLS and crystallinity of the PE have not been studied before. The objective of this study is, therefore, to investigate the mechanical properties and non-linear creep behavior of polyethylene MLS nanocomposites and correlate the response to MLS dispersion and crystallinity in the films.

1.1. Creep modeling with mechanical analogs

Creep deformation is the time dependent strain under constant stress. Creep modeling and analysis is important from a fundamental and application driven perspective. The determination of the time response enables analysis of chain dynamics. Stress applied on a viscoelastic material is time and temperature dependent. The rheological response of a purely elastic material is instantaneous while that of viscoelastic material is time dependent [24]. Many models exist to describe the viscoelastic creep response of polymers. Each model comprises of a spring and a dashpot connected in a variety of configurations and has its own limitations. Mechanical analogs to electric circuits include the Maxwell model, Kelvin model, Burger model, and generalized Maxwell and Kelvin model. Molecular models such as Kohlrausch–Williams–Watts (KWW) model, and power law models have also been used. KWW has been found to be valid for creep over limited periods of time [24,25]. In the case of a Burger model (Fig. 1), the strain is equal to strain in the Maxwell model and Kelvin model.

$$\gamma_B = \frac{\sigma}{E_M} + \frac{\sigma}{E_K}\left[1 - \exp\left(\frac{-E_K t}{\eta_K}\right)\right] + \frac{\sigma t}{\eta_M} \quad (1)$$

where E_M, η_M is elastic and viscous component of Maxwell model. E_K, η_K is elastic and viscous component of Kelvin model [26]. In the case of the creep step (Fig. 2), when the force F is applied, the Maxwell spring S_1 initially deforms. The Kelvin spring S_2 and dashpot D_2 show a delayed deformation at longer times followed by continuous deformation of dashpot D_3. When the applied force is removed (recovery step), the Maxwell spring S_1 recovers completely. The Kelvin spring S_2 and dashpot D_2 show delayed deformation while dashpot D_3 remains permanently deflected. We can divide the curve into three regions. γ_e is the purely elastic deformation in spring S_1 occurring immediately after application of a load (Maxwell model). γ_K is the delayed viscoelastic deformation of spring S_2 together with dashpot D_2 (Kelvin model). γ_n is the purely viscous deformation of dashpot D_3 (Maxwell model). The maximum strain experienced by a polymer in a Burger model is the addition of γ_e, γ_K and γ_η [26].

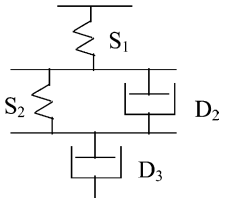

Fig. 1. Schematic of the Burger 4 element model.

2. Experimental

2.1. Materials

PE (MI ~ 1.0 gm/10 min and density ~0.96 gm/cc) of Huntsman LLC was used to make the PE–MLS nanocomposite films. Montmorillonite layered silicate clay of the Cloisite family (Cloisite 15A™) was obtained from Southern Clay. A maleated PE (PE-*g*-MA) of SMI Technology was used as a coupling agent between the layered silicate and the PE matrix. The parameters investigated were the ratio of PE-*g*-MA:MLS, separation of effects due to PE-*g*-MA or due to MLS and increased

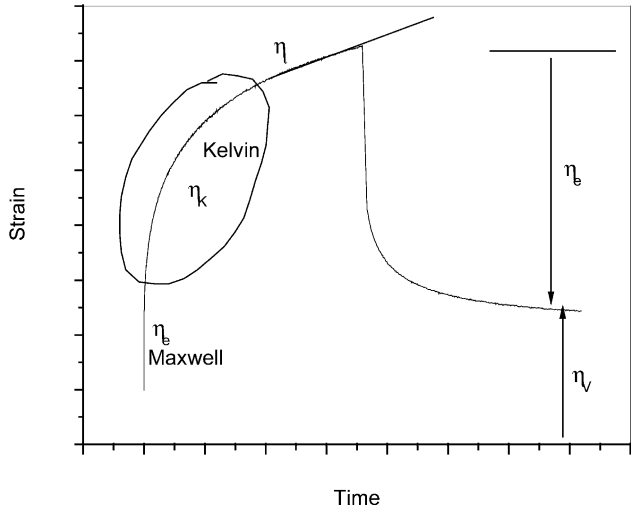

Fig. 2. Creep-recovery strains corresponding to the individual elements of the Burger model.

fraction of MLS. Eight different batches were made with varying concentration of MLS and PE-*g*-MA. Table 1 gives the ratios of the different blends. The effects of PE-*g*-MA and MLS were individually investigated through addition of individual components. The effects of the combined MLS + PE-*g*-MA systems were investigated by adding the 1:1 blends of MLS and PE-*g*-MA at 1, 2, 5 wt% into PE. Also to separate the effects of PE-*g*-MA from MLS, the blends of PE with MLS (at 2.5 and 5 wt%) were included in this study.

All the formulations (Table 1) were compounded by a Haake TW100 twin screw extruder with a temperature profile of 390, 390, 400, and 410 F for zones 1–4. PE films (1 mm thick) were produced by a Killion single screw extruder ($L/D = 24:1$), fitted with a dual lip air ring and die of 2-in. diameter from all the formulations. Since, MLS exhibits affinity to moisture, it was dried for almost 48 h in a forced air convection oven at 60 °C prior to preparing the master-batch of MLS and PE-*g*-MA. To prepare the PE + MLS systems, a master batch of PE and MLS (25%) was extruded and pelletized. Appropriated PE levels were then added and the mixture re-compounded and pelletized. The pelletizer was then removed and a blown film die was used to manufacture film with a take up speed of 7.62 m/min. Blends of PE + MLS + PE-*g*-MA were made using a master batch of MLS (25 wt%) and the PE-*g*-MA (25 wt%). Pellets of the master-batch were introduced into the base PE resin to achieve appropriate concentrations of MLS and PE-*g*-MA. The compounded pellets were then blown film processed.

2.2. Mechanical testing

Tensile and creep testing was done on a Rheometric Scientific Instrument (RSA III) with a film tool attachment. ASTM D882-02 was used to measure tensile properties of thin PE films. Creep tests were done at two stress levels corresponding to 25 and 50% of the yield stress for the corresponding samples. The films were loaded for 1 h and then the recovery was measured for 1 h at ambient temperatures.

Table 1
Compositions examined

ID	PE (wt%)	PE-*g*-MA (wt%)	MLS (wt%)
A	100	–	–
B	99	1	
C	99		1
D	97.5		2.5
E	95		5
F	98	1	1
G	95	2.5	2.5
H	90	5	5
I	92.5	5	2.5

2.3. Differential scanning calorimetry (DSC)

Thermal characterization of PE–MLS nanocomposites was performed using a Perkin–Elmer DSC6. The system was calibrated using indium and zinc. 5–10 mg of sample was taken from 30 to 170 °C at 10 °C/min. Samples were annealed for 30 min and then slow cooled down. Subsequent melting scans were also analyzed. All samples were done under nitrogen.

2.4. X-ray diffraction (XRD)

XRD was carried out on 1 m thick samples. A Siemens D500 X-ray diffractometer was used to study the dispersion behavior and PE crystallinity. The scanning angle for all the experiments was kept between $2\Theta = 2$ and 70° and a step size of 0.02.

2.5. Polarized optical microscopy (POM)

POM was conducted on a Zeiss optical microscope. The lens magnification was 40×. An INSTEC hot stage was used to heat and cool samples in a microscope. Samples were heated above melting point and cooled very slowly (1 °C/min) to study the crystallinity of PE. The pictures were taken using CONTAX camera.

3. Results and discussions

3.1. Instantaneous mechanical response-tensile test results

Fig. 3 shows the overlay of stress–strain curves of films, which were analyzed, and results tabulated in Table 2. When PE-*g*-MA (sample B) was added to the PE, a

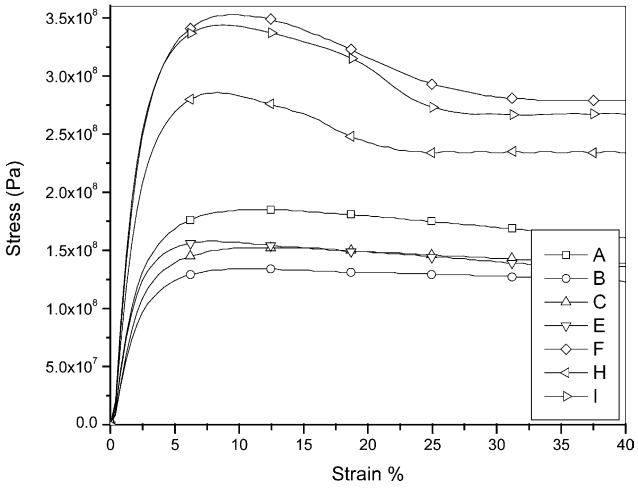

Fig. 3. Tensile stress–strain curves of the films showing decreased performance in PE-*g*-MA:MLS samples alone and synergistic benefits in the combined system.

Table 2
Mechanical properties of polyethyelene and nanocomposite films

Film	UTS (MPa)	Yield (MPa)	Modulus (GPa)
A	26	15	0.58
B	13	10	0.46
C	16	10	0.5
D	17	10	0.65
E	18	11	0.8
F	35	18	1.4
G	27	19	1.1
H	27	20	0.89
I	31	24	1.3

significant drop in modulus and UTS is evident. Adding 1, 2.5 and 5% MLS (samples C–E) to PE resulted in the UTS and modulus increasing with concentration but the values are lower than the original PE. The combined PE + PE-*g*-MA + MLS nanocomposites (samples F–I), however, show a synergistic effect for all mechanical properties. The stress–strain curves show evidence of significant yielding followed by post-yield drop when MLS and PE-*g*-MA are compounded together with PE. The highest UTS and yield strength were obtained for a 1% addition of both MLS and PE-*g*-MA. Significantly, the addition of PE-*g*-MA improved properties relative to the PE modified with MLS alone at the same loading (sample C vs. F and D vs. G) When a higher level of MLS (2.5 and 5%) was added to PE-*g*-MA in a 1:1 ratio, the UTS and yield dropped but the modulus increased. Comparing the 1:1 sample of 2.5% ML to the 5% MLS (samples G and H), there is no distinction between the UTS, yield strength and modulus of the films. When a 2:1 ratio of PE-*g*-MA to PE was analyzed, yield improved (sample I vs. G).

It is clear, therefore, that all maleated PE nanocomposites (PE-*g*-MA + PE + MLS) films showed an increase in modulus compared to neat PE compared to films made without the maleated PE. The results indicate a synergistic contribution of both MLS and PE-*g*-MA when added together. The films had a high strain to failure, exceeding the measurement extension of our MTS (5 in.) The samples remained plastically deformed within the test fixtures. The PE nanocomposite films without PE-*g*-MA showed poor overall mechanical properties. On an average there was a 60% drop in UTS compared to neat PE for PE nanocomposite films without the maleated PE coupling agent. The same trend was observed for modulus and yield stress, where properties were observed to be inferior to neat PE.

3.2. Creep response and Burger analysis

Fig. 4 shows the creep behavior of PE nanocomposites at stresses corresponding to 50% yield stress of each material. All the stress values were calculated by doing tensile tests of individual films. All the samples showed permanent irrecoverable strain even though the applied load was well within the linear region. This behavior shows the non-linear behavior of all films.

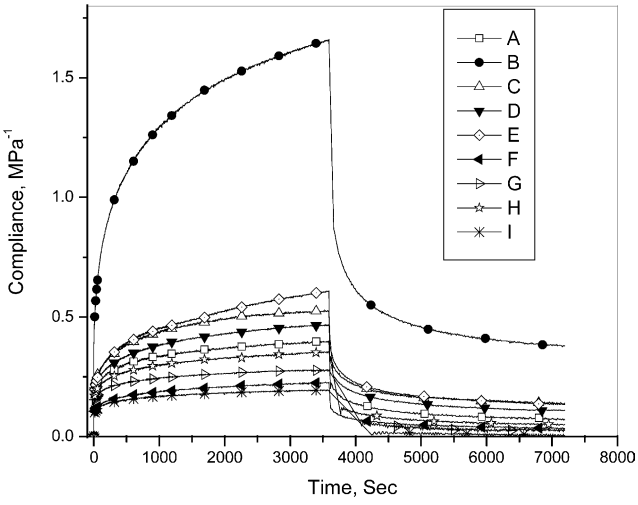

Fig. 4. Creep-recovery measurements of the films.

When PE-*g*-MA is added to PE, the creep compliance is significantly greater than that of PE while when MLS is added, the compliance decreases relative to the host PE. Significantly while the initial compliance decreases with increasing MLS concentration, the time dependent compliance increases. A combined MLS + PE-*g*-MA in a 1:1 ratio shows that at low MLS concentrations the creep compliance is the lowest. With increasing clay concentration, the creep compliance over time increases. The percent recovery scales inversely with compliance.

Tables 3 and 4 display the Burger model parameters corresponding to 25 and 50% yield stress determined from the tensile data for each film. It is clear that all the fit parameters are greater in the MLS + PE-*g*-MA films compared to when there is no PE-*g*-MA. The MLS + PE-*g*-MA maleated PE nanocomposites also showed an increase in Maxwell elastic modulus (E_M). An increase in E_M is a direct indication of improvement in the elastic properties of material, which mirrors the tensile results. Most significantly, the % recovery was much higher in the maleated PE nanocomposites compared to the non-maleated nanocomposites. Under creep, more the elasticity more is the likelihood of recovery. Non-maleated nanocomposites did not show much improvement compared to neat PE. The trends were similar at 25 and 50% of yield stress values. The Kelvin parameters in the Burger model were analyzed to determine the retardation time. Ideal elastic materials display an immediate recovery after loading and subsequent removal of the load. In the case of viscoelastic materials, there is a time delay for recovery. Retardation time is the delayed response to an applied force or stress. Fig. 5 displays the retardation time behavior of PE nanocomposites. Maleated PE nanocomposites showed smaller retardation time compared to non-maleated nanocomposites. Both E_M and retardation time reflect the final percentage

Table 3
Burger analysis at 25% yield stress of PE nanocomposites

	E_M (MPa)	E_K (MPa)	η_K (MPa s)	η_M (MPa s)	% Recovery
A	5.6	8.0	2400	58,000	80
B	3.8	6.9	1800	38,000	86
C	3.7	7.0	1200	30,000	73
D	5.0	7.0	1500	27,000	74
E	5.2	5.0	700	24,000	79
F	10.2	13.0	1500	55,000	84
G	9.0	9.0	1200	95,000	83
H	7.0	13.0	1900	60,000	87
I	8.8	13.8	1500	68,000	85

Table 4
Burger analysis at 50% yield stress of PE nanocomposites

	E_M (MPa)	E_K (MPa)	η_K (MPa s)	η_M (MPa s)	% Recovery
A	5.5	7.0	2300	33,000	79
B	1.8	1.6	500	7300	74
C	5.0	5.0	1300	26,500	72
D	7.0	7.4	1900	32,000	75
E	4.9	5.0	1500	18,000	78
F	11.5	15	2800	54,000	85
G	11.0	15.7	2500	66,200	86
H	9.6	12.0	2000	69,000	85
I	12.0	15.0	1900	75,000	88

recovery of all PE nanocomposites. Burger fits of PE nanocomposites are shown in Fig. 6. It is clear that all maleated nanocomposites showed better creep properties than non-maleated samples.

To correlate the synergistic effects of MLS and PE-*g*-MA in PE to morphological changes, crystallinity changes in the PE in the different systems were investigated using the DSC, POM and XRD. Struik proposed a model to understand the mechanism of plastic deformation even under low stresses [27]. His model is based on the separation of a semicrystalline polymer into three regions: the crystalline region, the amorphous region next to crystalline region and the complete amorphous region. Below the glass transition temperature, the amorphous phases will be glassy and the material will show the same aging behavior as a purely crystalline polymer. Above the glass transition temperature, the amorphous chain segments have significant mobility resulting in unrecoverable creep induced strains. Thus above the glass transition temperature and below the melting temperature, the amorphous segments far from the

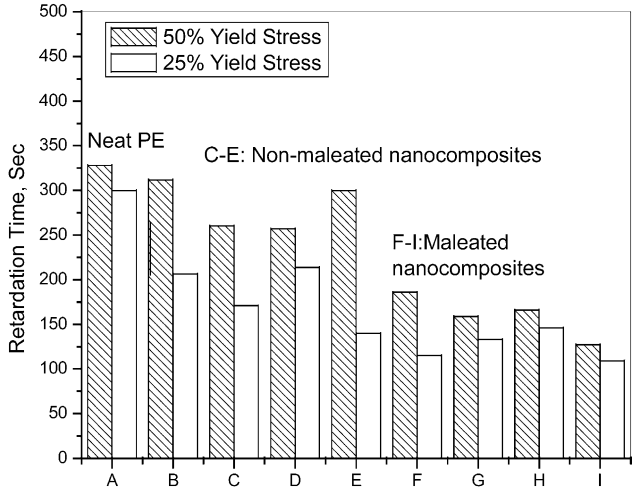

Fig. 5. Retardation time of the nanocomposites for 25 and 50% of yield stresses showing similar trends.

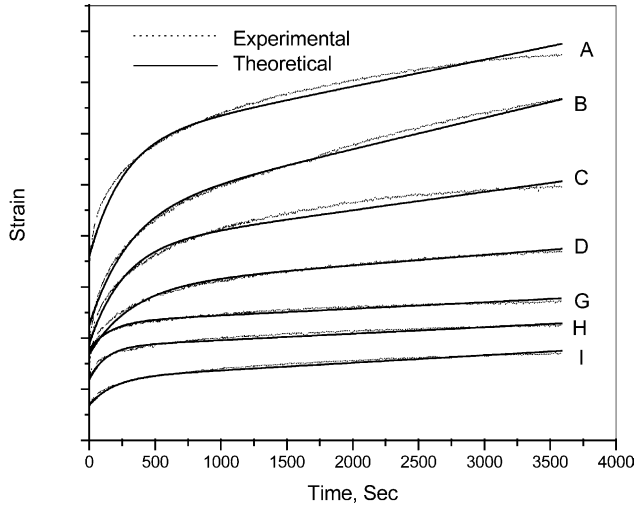

Fig. 6. Experimental and predicted creep curves for the films.

crystallites are significantly mobile. The crystalline regions display linear behavior while non-linearity occurs due to the amorphous segments.

Figs. 7 and 8 show the DSC melting and recrystallization curves of the films. PE and PE nanocomposites showed two melting peaks during heating. The broad melting curve in the PE film is made more pronounced in the combined PE-*g*-MA + MLS films. The origin of the doublet in the melting peaks may be explained by the presence of two populations of crystallites of different thermal stability. Double melting peaks are also an indication of a high degree of branching found in LLDPE. Less branched molecules form more stable crystals and crystallize at a higher temperature. Since, the doublets existed both in the as-processed sample and in the post annealed MLS modified samples, the result indicates that a bimodal crystallite population results from MLS addition. The enthalpies of melting (Table 5) indicate that when PE-*g*-MA or MLS are individually added to PE, the enthalpies of melting are significantly higher than that of the films containing both additives. The enhancement of heats of fusion in the PE + PE-*g*-MA materials are mimicked by the PP + PP-*g*-MA systems and have been attributed to changes in crystal density [28]. There is no discernable change in both melting and recrystallization peaks and the initial slopes of the recrystallization peak are similar for all samples. We have previously shown heterogeneous nucleation by MLS in nylon system, where the addition of MLS changed the recrystallization temperature by 20 °C [29]. The recrystallization peak of all PE samples showed the same onset temperature (±2 °C). The similar slope and onset temperatures indicated no heterogeneous nucleation effect of MLS in PE. The addition of MLS had no effect on the recrystallization temperature but the width of the transition was affected. The width of the transition was considerably higher for all samples containing PE-*g*-MA. Comparing PE + MLS composition with and without PE-*g*-MA, a significant increase in the FWHM in all maleated nanocomposites is seen. The effect was concentration independent. The results indicate that while there is no marked change on the melting and recrystallization temperatures, the combined PE-*g*-MA + MLS samples has a wider distribution of crystallite sizes and decreased overall crystallinity reflected in lower enthalpies of melting and recrystallization. This crystallite dimensional effect was also probed by XRD. The diffraction pattern of PE has two characteristic peaks (110) and (200) at $2\Theta = 21$ and 24°. Addition of PE-*g*-MA showed no shift in the peak position indicating no structural change in the PE (Table 6). Scherrer's equation was used to calculate the crystalline thickness perpendicular to the reflection plane.

Table 5
DSC results of the films

Sample	T_m (°C)	H_m (J/g)	T_c (°C)	H_c (J/g)
A	135.3	176.1	118.5	170.4
B	133	297.6	117	303
C	134	202.7	117.5	291.6
D	134.2	253.4	117.6	265
E	134.6	258.9	116.9	245.6
F	135.6	183.2	118.5	180.3
G	135.5	161.6	118.5	154.3
H	134.4	144.8	118.5	143.5
I	135.2	187.3	118.8	186.8
PE-*g*-MA	130.9	190.9	109.2	195.5

$$L_{hkl} = \frac{K\lambda}{\beta \cos \theta} \tag{9}$$

where θ is Bragg's angle, β is the FWHM of diffraction peak in radians, K equal to 0.9, and λ is the wavelength of the X-ray (nm). The addition of MLS increased the crystalline

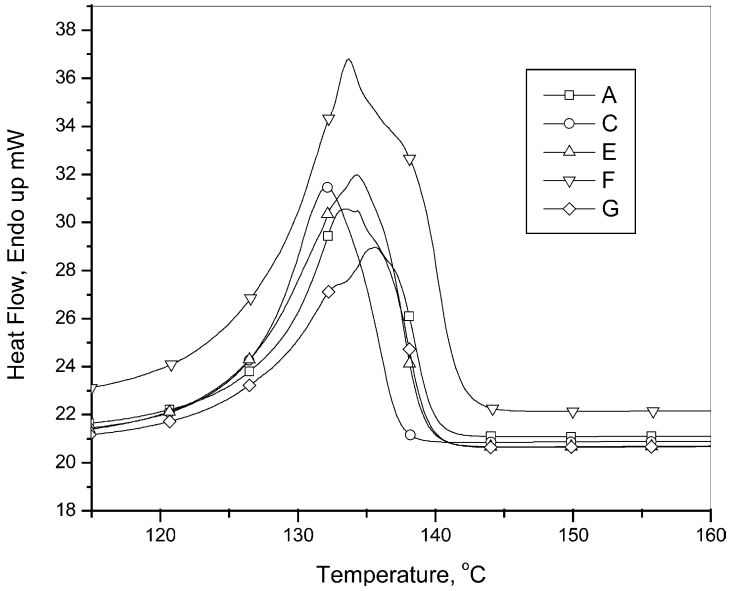

Fig. 7. Melting curves of the films showing peak doublet in the base film and nanocomposites.

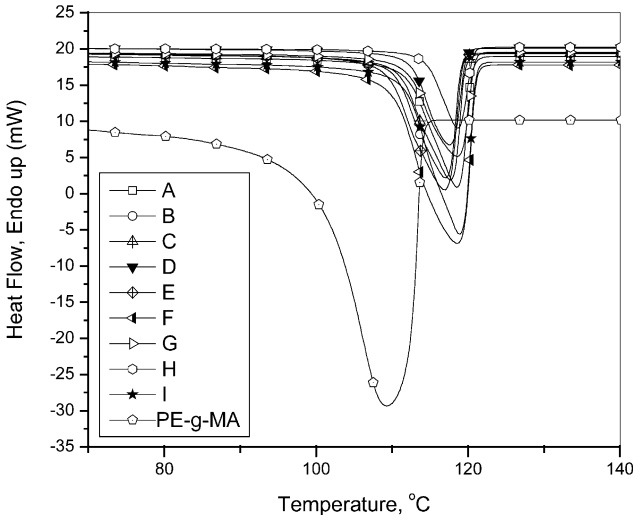

Fig. 8. Recrystallization curves of the films showing little change in onset temperatures and slope.

lamella thickness perpendicular to reflection plane from 24 to 29 nm for (110) peak. Though the change in crystalline thickness was not significant, there was some indication of the effect of MLS on the growth of PE crystallinity. We attribute that to the lower concentration of PE-*g*-MA (maximum 10% by weight) used in our films. In previous work, Liang et al. [30] observed significant difference in the crystalline thickness of maleated HDPE nanocomposites at very 10% PE-*g*-MA concentrations using XRD. At 15% by weight of PE-*g*-MA and 3% by weight MLS, the crystalline thickness of (110) and (200) planes dropped by 50 and 62%, respectively. At a lower percentage of PE-*g*-MA (9%), the drop in crystalline thickness was only 10%. The drop in crystalline thickness was related to imperfections in crystals due to presence of MLS and PE-*g*-MA and was related to heterogeneous nucleation. Liang et al. [30] predicted that a minimum 10% of PE-*g*-MA was required to see the heterogeneous nucleation effect in PE nanocomposites. Since, our films had a lower amount of maleated PE (5% maximum by weight), we did not see a dramatic drop in crystalline thickness. However, we have determined a marginal increase in crystalline thickness of 10% for (110) and 16% for (200) plane. The effect was the same regardless of the presence or absence of PE-*g*-MA. Fig. 9(a)–(c) show the polarized optical micrograph of neat polyethylene, maleated nanocomposite and non-maleated nanocomposite, respectively. Neat PE showed an average crystallite diameter of 5.7 μm. The addition of MLS increased the average diameter of spherulite by a factor of two. Table 7 shows the crystallite size comparison in all PE nanocomposites. The effect was concentration independent. Both maleated and non-maleated PE nanocomposites showed the same average increase in crystallite size. Given that the DSC melting and fusion temperatures showed no change, this could imply that the smaller crystallites had a smaller population than the larger crystallites in the host PE resin. Most critically, we determine that the decreased melting enthalpies in the nanocomposites containing maleated PE compared to nanocomposites with no maleated PE negates the possibility that increased crystallinity could be responsible for improved mechanical properties. We hypothesized that the MLS rigid platelets, tethered via the reactive surfactants to the host matrix would mimic rigid crystals and could act as anchors to the polymer matrix. To determine if dispersion of the MLS was the key contributor to the improved tensile and creep performance, we investigated the nano and mesoscale dispersion of the platelets. Fig. 10 shows the X-ray diffraction pattern of some films. The MLS used in PE system has three characteristic peaks at low $2\Theta = 2.7°$ (001), 4.3° (002) and 7.1° (003) which corresponds to a basal spacing of around 32A, 20A, and 12A° for (001), (002) and (003) peak, respectively. Comparing the diffraction spectra of the 1 and 2.5% MLS films with and without PE-*g*-MA, it is apparent that PE-*g*-MA suppresses the peak intensity of the MLS interlayer basal spacing peak. We studied the degree of disorder (full width half maximum (FWHM)) at different concentrations in the PE matrix values of the characteristic (001) peaks. The results are shown in Table 6. Increase in FWHM values for PE nanocomposites compared to pure MLS showed an increase in structural disorder

Table 6
XRD of the films showing the changes in the PE crystallite dimensions for combined PE-*g*-MA + MLS films compared to individually compounded films

	Crystalline thickness (nm)	PE (110), 2Θ	Crystalline lamella thickness (nm)	MLS (001), 2Θ	FWHM, MLS (001)
MLS				2.7	0.68
A	24.0	21.6	18.0		
B	24.1	21.8	19.0	2.5	–
C	26.1	21.6	20.1	2.6	0.76
D	28.8	21.6	21.2	2.7	0.80
E	29.0	21.6	21.5	2.8	0.87
F	25.0	21.6	19.8	2.4	No full peak
G	26.2	21.9	20.4	3.0	0.78
H	27.5	21.9	21.0	3.0	0.72
I	28.0	21.6	22.0	3.1	0.75

Data for the MLS (001) peak is also shown.

Table 7
Size of clay agglomerates and spherulite size observed during optical analysis

	MLS size (μm)	Average spherulites size (μm)
A	–	5.7
B	–	5.8
C	4.65	11.62
D	5.15	10.68
E	5.19	10.75
F	2.33	11.68
G	2.50	11.12
H	3.21	11.0
I	3.16	11.30

within silicate layers. It was also observed that increase in PE-*g*-MA:MLS ratio had no effect on the width of the MLS peak. While the PE-*g*-MA did not facilitate exfoliation or intercalation of the MLS, the results indicate some favorable interaction. The polar groups of the PE-*g*-MA facilitate favorable interactions to the clay surfactant molecules resulting in a higher FWHM. At the mesoscale, however, dispersion is favored in the combined PE-*g*-MA + MLS films. Fig. 11(a) and (b) show the optical micrograph of 5% MLS PE nanocomposites with and without PE-*g*-MA, respectively, (samples E and H). Optical micrograph of 5% MLS nanocomposite with PE-*g*-MA shows small MLS agglomerates. As discussed before, layered silicates have thickness of 1 nm and lateral end-to-end distance of 1–1 μm. All maleated nanocomposites showed average size ranging from 2.3 to 3.2 μm. This size reflects lateral silicate layers forming a group. PE nanocomposites without PE-*g*-MA showed bigger silicate groups of average diameter of 4.5–5 μm. The bigger size reflects lower disorder within silicate galleries [31].

It is clear, therefore, that the distribution of MLS into the PE film is facilitated by the PE-*g*-MA. For the same concentration of MLS, the lower degree of agglomeration resulting from PE-*g*-MA addition enables a higher interfacial area and more effective use of the MLS. The agglomeration results in a macro-composite that results in lower mechanical properties in all the PE + MLS films without PE-*g*-MA. In keeping with Struik's analysis of the impact of crystalline domains in an amorphous matrix, we determine that the MLS acts as a crystalline domain restricting the mobility of the PE chains when it has a low level of agglomeration. This results in lower creep compliance over time and higher strain recovery compared to the agglomerated dispersion.

We attribute the increase in mechanical and creep behavior to better dispersion in maleated nanocomposites compare to non-maleated nanocomposites. Low molecular weight MA served as a perfect coupling agent by forming a good dispersed nanocomposite system.

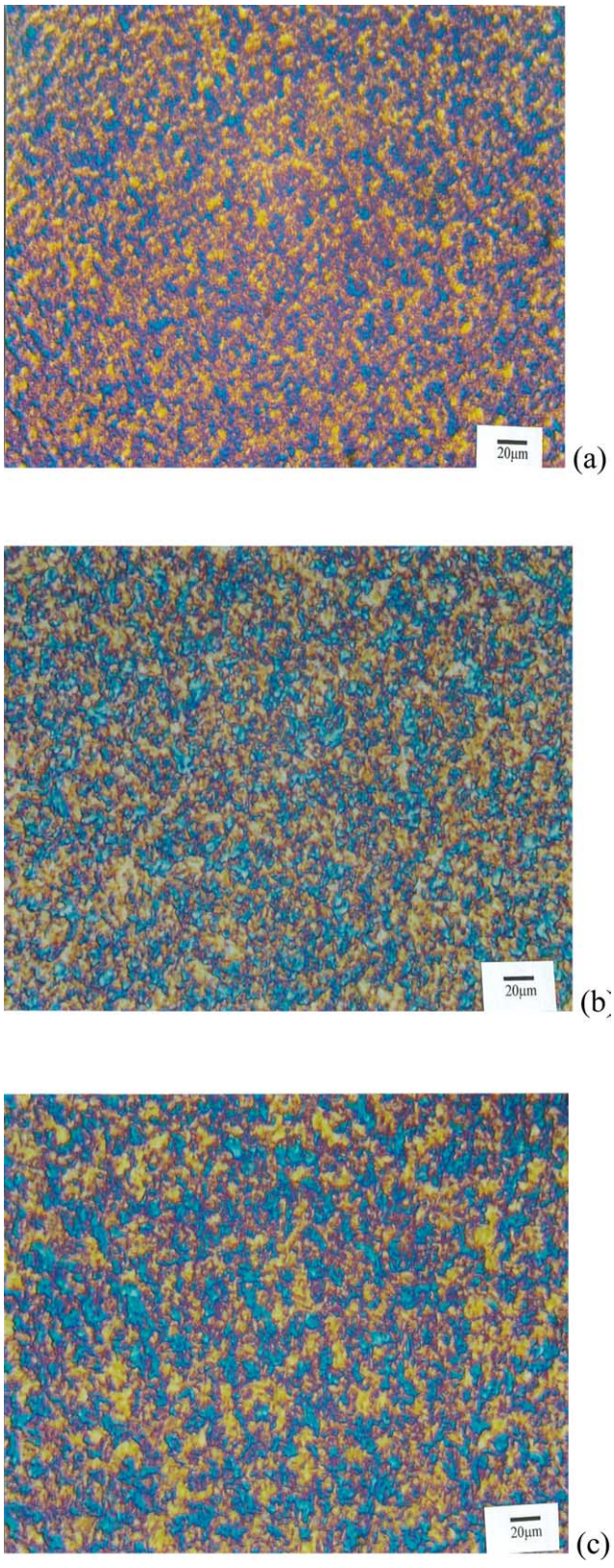

Fig. 9. Polarized optical micrographs of (a) sample A (b) sample G and (c) sample C.

4. Conclusion

PE-*g*-MA facilitated the dispersion of the MLS in PE

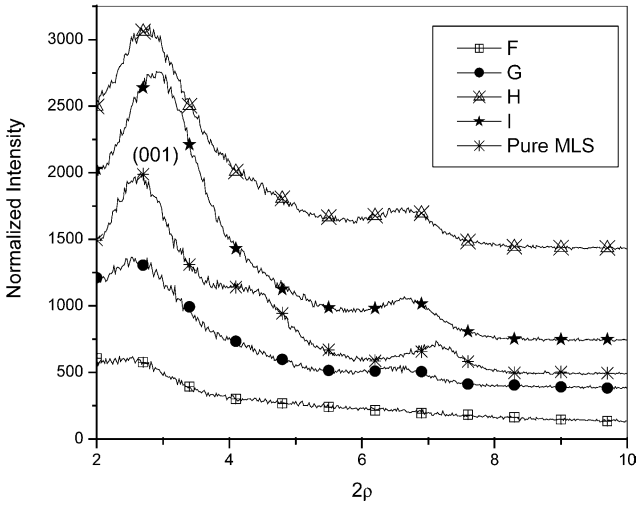

Fig. 10. XRD of some films showing that the peak maxima was unaffected by composition but the breadth and the intensity showed some effect.

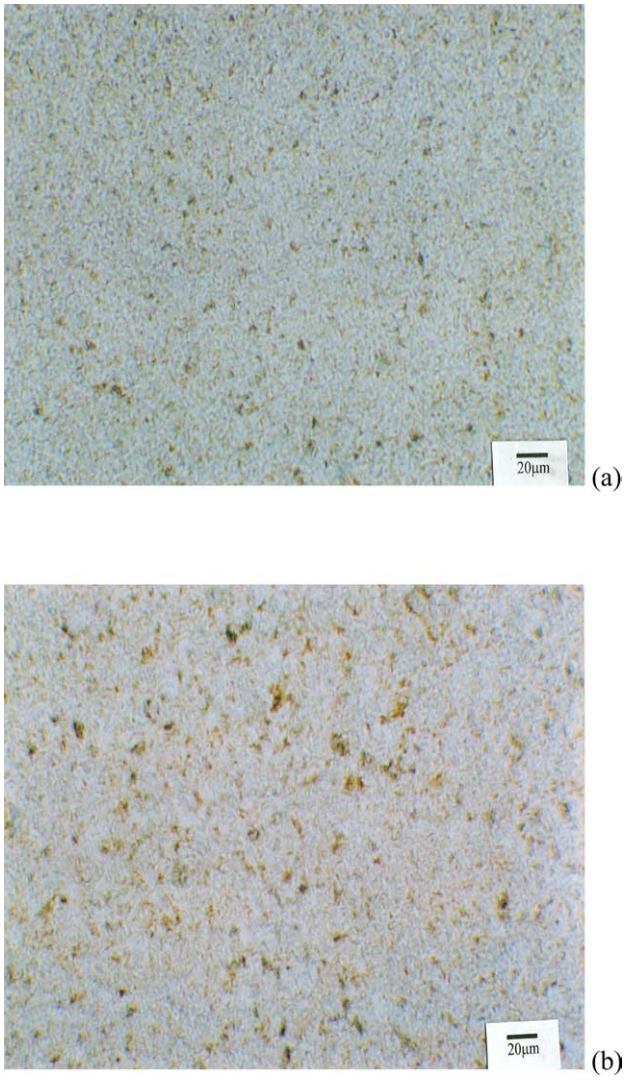

Fig. 11. POM of sample E (a) and sample H (b) showing smaller clay aggregates in the maleated PE modified films.

resulting in synergistic improvements in the creep-recovery and mechanical properties of the films. The Burger model was successfully used to analyze the non-linear behavior of PE nanocomposites. Maleated nanocomposites showed higher UTS and yield strength compared to non-maleated nanocomposites. Maleated nanocomposites also showed increase in modulus over neat PE. The Burger analysis revealed a decrease in retardation time for maleated nanocomposites compare to non-maleated nanocomposites. Maleated nanocomposites showed an increase in stored energy, which reflected into increase in elastic modulus. Maleated nanocomposites also showed lower strain at UTS than neat PE. The increase in physical and creep properties in case of maleated PE nanocomposites was due to synergistic contributions from PE-*g*-MA and MLS. Presence of PE-*g*-MA improved miscibility between non-polar PE chains and MLS forming an intercalation. Non-maleated nanocomposites showed poor mechanical and creep properties reflecting the importance of PE-*g*-MA in the PE system. Diffraction analysis coupled with optical microscopy revealed a more uniform dispersion in maleated nanocomposites than in non-maleated nanocomposites. MA acted as a coupling agent between MLS and PE and the miscibility between MLS and PE was increased due to polar nature of MA. The improved creep response was correlated to the presence of rigid MLS and not significantly to changes in crystallinity. Maleated PE nanocomposites showed higher percent recovery than that of non-maleated nanocomposites. The compliance did not decrease linearly with increase in MLS concentration. We attribute this effect to the separate PE–PE-*g*-MA interactions, which dominated with increase in concentration of low molecular weight MA. Maleated PE nanocomposites not only showed better creep recovery but also showed lower creep strains than neat PE and non-maleated nanocomposites. The amorphous regions in PE, which are the primary cause for the non-linearity, experienced restricted chain movement and a higher resistance to deformation due to hard MLS platelets. The behavior remained somewhat the same even at higher MLS concentration.

Acknowledgements

The authors acknowledge financial support from NASA Wallops Flight Facility (Contract # NAG5-5352). We acknowledge Bert Powell at Southern Clay for his assistance in choosing the clay.

References

[1] Vaia RA. Polymer melt intercalation in mica-type layered silicates. PhD Thesis, Cornell University, USA; 1995.
[2] Pinnavaia TJ, Beall GW. Polymer clay nanocomposites. New York: Willey; 2001.

[3] Kojima Y, Fukumori K, Usuki A, Okada A, Kurauchi T. J Mater Sci Lett 1993;12:889.
[4] Vaia R, Giannelis P. Macromolecules 1997;30:8000.
[5] Galgali G, Ramesh C, Lele A. Macromolecules 2001;34:852.
[6] Gu S, Ren G, Wang Q. J Appl Polym Sci 2004;91:2427.
[7] Lim S, Lee C, Choi H, Jhon M. J Polym Sci, Part B: Polym Phys 2003; 41:2052.
[8] Pegoretti A, Kolarik J, Peroni C, Migliaresi C. Polymer 2004;45(8): 2751–9.
[9] Lee A, Lichtenhan J. J Appl Polym Sci 1999;73:1993.
[10] Lai J, Bakker A. Polymer 1995;36:93.
[11] Hernandez-Luna A, D'Souza NA. ANTEC Proc 2002;1461.
[12] Ward IM. Macromol Symp 1998;1029.
[13] Wilding M, Ward M. Polymer 1981;22:870.
[14] Fotheringham D, Cherry R. J Mater Sci 1978;13:951.
[15] Zhang C, Moore ID. Polym Eng Sci 1997;37:404.
[16] Zhang C, Moore ID. Polym Eng Sci 1997;37:414.
[17] Suwanprateeb J, Tanner KE, Turner S, Bofield W. J Mater Sci Mater Med 1995;6:804.
[18] Rand JL, Grant DA. Polym Eng Sci 1996;36:1058.
[19] Schapery RA. Polym Eng Sci 1969;9:295.
[20] Zhou H, Wilkes G. Polymer 1998;39:3597.
[21] Xu B, Rochefort EE. J Appl Polym Sci 2000;76:1100.
[22] Hubert L, David L, Germain Y. J Appl Polym Sci 2000;84:2308.
[23] Drozdov AD, Christiansen JC. Polymer 2002;43:4745.
[24] Aklonis J, MacKnight W. Introduction to Polymer Viscoelasticity. New York: Wiley; 1983.
[25] Read RE. J Non-Cryst Solids 1991;408:131.
[26] Mezger T. The Rheology Handbook. Hannover, Germany: Vincentz-Verlag; 2002.
[27] Struik LCE. Physical aging in amorphous polymers and other materials. New York: Elsevier; 1978.
[28] Kilwon C, Li L, Choi J. Polymer 1999;40:1719.
[29] Ranade A, D'Souza N, Gnade B, Dharia A. J Plast Film Sheeting 2003;19:271.
[30] Liang G, Xu J, Bao S, Xu W. J Appl Polym Sci 2004;91:3974.
[31] Ranade A, D'Souza N, Gnade B. Polymer 2002;43:3759.